Dynamic evolution of a hydraulic-mechanical-electric system with randomly fluctuating speed based on Chebyshev polynomial approximation method

Beibei Xu[a], Diyi Chen*[a,b], Caraballo, Tomas[c]

[a]*Institute of Water Resources and Hydropower Research, Northwest A&F University, Shaanxi Yangling 712100, P. R. China*

[b]*Key Laboratory of Agricultural Soil and Water Engineering in Arid and Semiarid Areas, Ministry of Education, Northwest A & F University, Shaanxi Yangling 712100, P. R. China*

[c]*Depto. Ecuaciones Diferenciales y Análisis Numérico, Facultad de Matemáticas, Universidad de Sevilla, c/ Tarfia s/n, E-41012 Sevilla, Spain*

Corresponding author: Diyi Chen
Mailing Address: Institute of Water Resources and Hydropower Research, Northwest A&F University, Shaanxi Yangling 712100, China
Telephones: 086-181-6198-0277
E-mail: diyichen@nwsuaf.edu.cn

Abstract The research proposed in this paper focuses on the dynamic evolution of a hydraulic-mechanical-electric system under the effect of randomly fluctuating speed. The rapid growth of installed wind power capacity may potentially affect the stability of power grids, causing larger fluctuations of the generator speed to hydropower stations. In this work, a probabilistic component is associated to the generator speed of a deterministic hydraulic-mechanical-electric system providing a novel random model. This latter is analyzed to investigate the dynamic evolution of the system adopting the Chebyshev polynomial approximation method. A careful comparison of the numerical application results obtained by the deterministic and the probabilistic approaches is carried out. In addition, the influence of the fluctuation intensity (D) on the differential gain (k_d) of

the PID is investigated, proposing a law for k_d as function of D. Finally, the operating ranges of the grid water hammer and of the elastic water hammer models are compared in order to validate the consistence of the law. The results of the study provide robust bases for the stable and safe operation of hydropower stations.

Key words: vibration characteristics; hydraulic-mechanical-electrical system; randomly fluctuating generator speed; elastic water hammer; Chebyshev polynomial approximation;

1. Introduction

Over the last decades, the hydropower sector has experienced a rapid development in China, with the constructions of power stations in every corner of the country, reaching an installed capacity of ten hundred million kilowatts [1-4]. Furthermore, according to the 2014 plan agreed by most international hydropower industries, the construction of new hydropower installations will be promoted in order to double the worldwide installed capacity within the next thirty years [5, 6]. Due to this rapid expansion, the reliability and safety of such installations have nourished the concerns of the public opinion as well as of the regulators [7-12]. In particular, the hydraulic-mechanical-electrical system is a crucial component which plays an essential role for the safety of individual installations and can hence affect the stability of the whole electric power grid. Therefore, the analysis of the stability of hydraulic-mechanical-electric systems is a high-priority topic of research. In spite of this, the scientific literature in this field is still quite limited. Studies focusing on hydraulic-mechanical-electric systems can be roughly classified in two groups. The first focuses on the grid water hammer theory, aiming at establishing deterministic models for the hydraulic-mechanical-electric system [13-16]. This approach is suitable to describe the dynamic evolution of hydropower stations with short penstocks characterized by uniform geometry. The works belonging to the second group adopt the elastic water hammer theory for the definition of the

determinist model [17-25]. This approach is used to accurately analyze the dynamic characteristics of hydropower stations with long penstocks and allows to take into account eventual shape changes in the geometry of the penstock.

In addition to water power, renewable energy includes solar, wind, geothermal or tidal power amongst others [26-31]. Moreover, as highlighted by the last Global Wind Energy Outlook, the wind power sector has grown rapidly over the last decades in terms of both technological and commercial competitiveness: this is expected to result in an installed capacity of nearly 2 TW by 2030, supplying between 16.7% and 18.8% of global electricity [32]. Obviously, this trend may potentially affect the stability of power grids, leading to larger random fluctuations of hydro-turbine generators speed [33-36]. High-intensity random fluctuations can lead to the breaking of the torque balance of hydro-turbine generator units and hence threaten its operating stability. Lots of studies have focused on the increasing randomness of power grid. Therefore, the increasing generation capacity of wind power installations introduces new important challenges to the stable operation of hydropower stations of any size.

At light of this, our work proposes a novel approach to the stability analysis of the hydraulic-mechanical-electric system with respect to the existing literature. First, a probabilistic component u is integrated with the generator speed ω, obtaining a novel probabilistic model of the hydraulic-mechanical-electric system. Second, by comparing the dynamic evolutions of the deterministic and probabilistic approaches, the advantages and drawbacks of each method are identified. Third, a mathematical definition of the differential gain k_d for the PID in function of the fluctuation intensity D is proposed. Finally, the consistence of such definition is verified through a numerical application.

The content of this paper is organized as follows: Section 2 presents the nonlinear probabilistic

model of the hydraulic-mechanical-electric system. Numerical simulations along with detailed analysis of the results obtained are presented in Section 3. Conclusive remarks and discussions are included in Section 4.

2. Nonlinear random models of hydraulic-mechanical-electric systems

The hydraulic-mechanical-electric system considering the elastic water hammer model adopted in this study is shown in Eq. (1):

$$\begin{cases} x_1 = x_2 \\ x_2 = x_3 \\ x_3 = -a_0 x_1 - a_1 x_2 - a_2 x_3 + y \\ \delta = \omega_s \omega \\ \omega = \dfrac{1}{T_{ab}}[m_t - \dfrac{E_q^{'} V_s}{x_{d\Sigma}^{'}} \sin\delta - \dfrac{V_s^2}{2} \dfrac{x_{d\Sigma}^{'} - x_{q\Sigma}}{x_{d\Sigma}^{'} x_{q\Sigma}} \sin 2\delta - D_t \omega] \\ y = \dfrac{1}{T_y}(k_p(r-\omega) + k_i x_4 - k_d \omega - y) \\ x_4 = r - \omega \end{cases} \tag{1}$$

Details about the parameters in Eq. (1) can be found in Ref. [24].

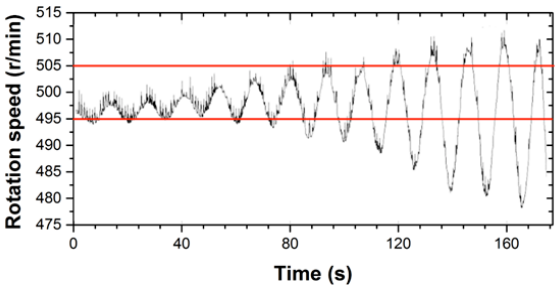

Fig. 1 Evolution in time of generator speed fluctuation

According to the nature of the fluctuation affecting the generator speed, two different types can be identified: the first refers to a limited range, of about 49.5~50.5 r/min, as shown in Fig. 1 for values of time *t* lower than 120 s. This type of fluctuation is difficult to detect from the generator running sound due to the negligibility of the associated noise compared to that of the operating environment. The second type refers to fluctuations within the range 49.5~50.5 r/min, as shown in Fig. 1 for time values *t* higher than 120 s. Both the types of identified fluctuation have the potential

to break the dynamic balance of torques between the hydro-turbine and the generator. In light of this, a probabilistic representation of the torque caused by the speed fluctuation is essential to obtain the state-space representation of the generator speed. Let $Du\omega$ be the random torque, then the generator speed can be written as:

$$\omega = \frac{1}{T_{ab}}\left[m_t - \frac{E_q^{'} V_s}{x_{d\Sigma}^{'}} \sin\delta - \frac{V_s^2}{2} \frac{x_{d\Sigma}^{'} - x_{q\Sigma}}{x_{d\Sigma}^{'} x_{q\Sigma}} \sin 2\delta - D_t\omega - Du\omega \right] \tag{2}$$

where u is the random variable introduced in this study. Its probability density function, shown in Fig. 2, can be described as [37]

$$p(u) = \begin{cases} \frac{2}{\pi}\sqrt{1-u^2}; & |u| \le 1. \\ 0; & |u| > 1. \end{cases} \tag{3}$$

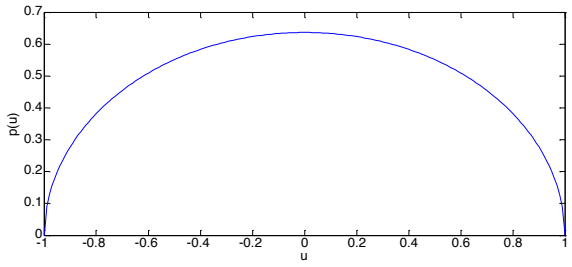

Fig. 2 The diagram of the probability density function $p(u)$.

Chebyshev polynomial approximation is used to simplify the probabilistic model of the hydraulic-mechanical-electric system. Such approximation can be presented as:

$$U_n(u) = \sum_{k=0}^{\frac{n}{2}} \frac{(-1)^k (n-k)!}{k!(n-2k)!} (2u)^{n-2k}. \tag{4}$$

Its recurrence relation is

$$nU_n(u) = \frac{1}{2}\left[U_{n-1}(u) + U_{n+1}(u)\right], \tag{5}$$

and the approximation property is

$$\int_{-1}^{1} \frac{2}{\pi}\sqrt{1-u^2} U_i(u) U_j(u) du = \begin{cases} 1, & i = j \\ 0, & i \ne j \end{cases} \tag{6}$$

According to the approximation theory of orthogonal polynomials and the above analysis, the random variables of the system can be written as

$$\begin{cases} x_1(t,u)=\sum_{i=0}^{N} x_{1(i)}(t)U_i(u) \\ x_2(t,u)=\sum_{i=0}^{N} x_{2(i)}(t)U_i(u) \\ x_3(t,u)=\sum_{i=0}^{N} x_{3(i)}(t)U_i(u) \\ \delta(t,u)=\sum_{i=0}^{N} \delta_{(i)}(t)U_i(u) \\ \omega(t,u)=\sum_{i=0}^{N} \omega_{(i)}(t)U_i(u) \\ y(t,u)=\sum_{i=0}^{N} y_{(i)}(t)U_i(u) \\ x_{4i}(t)=\sum_{i=0}^{N} x_{4i}(t)U_i(u) \end{cases}, \tag{7}$$

where N is the maximum number of Chebyshev polynomials; $x_{1(i)}(t)=\int_{-1}^{+1} p(u)x_1(t,u)U_i(u)du$;

$x_{2(i)}(t)=\int_{-1}^{+1} p(u)x_2(t,u)U_i(u)du$; $x_{3(i)}(t)=\int_{-1}^{+1} p(u)x_3(t,u)U_i(u)du$; $\delta_i(t)=\int_{-1}^{+1} p(u)\delta(t,u)U_i(u)du$;

$\omega_i(t)=\int_{-1}^{+1} p(u)\omega(t,u)U_i(u)du$; $y_i(t)=\int_{-1}^{+1} p(u)y(t,u)U_i(u)du$; $x_{4i}(t)=\int_{-1}^{+1} p(u)x_{4i}(t,u)U_i(u)du$.

At light of this, the random state-space equations of the hydraulic-mechanical-electric system can be rewritten as:

$$\begin{cases} \frac{d}{dt}\left[\sum_{i=0}^{N} x_{1(i)}(t)U_i(u)\right]=\sum_{i=0}^{N} x_{2(i)}(t)U_i(u) \\ \frac{d}{dt}\left[\sum_{i=0}^{N} x_{2(i)}(t)U_i(u)\right]=\sum_{i=0}^{N} x_{3(i)}(t)U_i(u) \\ \frac{d}{dt}\left[\sum_{i=0}^{N} x_{3(i)}(t)U_i(u)\right]=-a_0\sum_{i=0}^{N} x_{1(i)}(t)U_i(u)-a_1\sum_{i=0}^{N} x_{2(i)}(t)U_i(u)-a_2\sum_{i=0}^{N} x_{3(i)}(t)U_i(u)+\sum_{i=0}^{N} y_{(i)}(t)U_i(u) \\ \frac{d}{dt}\left[\sum_{i=0}^{N} \delta_{(i)}(t)U_i(u)\right]=\omega_s\sum_{i=0}^{N} \omega_{(i)}(t)U_i(u) \\ \frac{d}{dt}\left[\sum_{i=0}^{N} \omega_{(i)}(t)U_i(u)\right]=\frac{1}{T_{ab}}\left[m_t-P_e^{'}-\left(D_t+Du\right)\sum_{i=0}^{N} \omega_{(i)}(t)U_i(u)\right] \\ \frac{d}{dt}\left[\sum_{i=0}^{N} y_{(i)}(t)U_i(u)\right]=\frac{1}{T_y}(k_p(r-\sum_{i=0}^{N} \omega_{(i)}(t)U_i(u))+k_i\sum_{i=0}^{N} x_{4(i)}(t)U_i(u)-k_d\frac{d}{dt}\left[\sum_{i=0}^{N} \omega_{(i)}(t)U_i(u)\right]-\sum_{i=0}^{N} y_{(i)}(t)U_i(u)) \\ \frac{d}{dt}\left[\sum_{i=0}^{N} x_{4(i)}(t)U_i(u)\right]=r-\sum_{i=0}^{N} \omega_{(i)}(t)U_i(u) \end{cases} \tag{8}$$

where $P_e^{'}=\frac{E_q^{'}V_s}{x_{d\Sigma}^{'}}\sin\left[\sum_{i=0}^{N} \delta_{(i)}(t)U_i(u)\right]-\frac{V_s^2}{2}\frac{x_{d\Sigma}^{'}-x_{q\Sigma}}{x_{d\Sigma}^{'}x_{q\Sigma}}\sin 2\left[\sum_{i=0}^{N} \delta_{(i)}(t)U_i(u)\right]$.

From Eq. (5), the following relationship can be obtained:

$$\begin{aligned} U_0^2(u) &= U_0 \\ 2U_0U_1 &= 2U_1 \\ 2U_1U_2 &= 2(U_3+U_1) \end{aligned} \tag{9}$$

Combining the expressions obtained so far, $Du(\mathrm{t})\left[\sum_{i=0}^{N}\omega_{(i)}(t)U_i(u)\right]$ can be simplified as:

$$Du(\mathrm{t})\left[\sum_{i=0}^{N}\omega_{(i)}(t)U_i(u)\right]=\frac{1}{2}D\sum_{i=0}^{N}\omega_{(i)}(t)\left[U_{i-1}(u)+U_{i+1}(u)\right]=\frac{1}{2}D\sum_{i=0}^{N}\left[\omega_{(i-1)}(t)+\omega_{(i+1)}(t)\right]U_i(u) \tag{10}$$

where ω_{-1}=0, and ω_{N+1}=0.

Replacing Eq. (10) into Eq. (8), the probabilistic model of the system can be written as:

$$\begin{cases} \frac{d}{dt}\left[\sum_{i=0}^{N}x_{1(i)}(t)U_i(u)\right]=\sum_{i=0}^{N}x_{2(i)}(t)U_i(u) \\ \frac{d}{dt}\left[\sum_{i=0}^{N}x_{2(i)}(t)U_i(u)\right]=\sum_{i=0}^{N}x_{3(i)}(t)U_i(u) \\ \frac{d}{dt}\left[\sum_{i=0}^{N}x_{3(i)}(t)U_i(u)\right]=-a_0\sum_{i=0}^{N}x_{1(i)}(t)U_i(u)-a_1\sum_{i=0}^{N}x_{2(i)}(t)U_i(u)-a_2\sum_{i=0}^{N}x_{3(i)}(t)U_i(u)+\sum_{i=0}^{N}y_{(i)}(t)U_i(u) \\ \frac{d}{dt}\left[\sum_{i=0}^{N}\delta_{(i)}(t)U_i(u)\right]=\omega_s\sum_{i=0}^{N}\omega_{(i)}(t)U_i(u) \\ \frac{d}{dt}\left[\sum_{i=0}^{N}\omega_{(i)}(t)U_i(u)\right]=\frac{1}{T_{ab}}\left[m_t-P_e-D_t\sum_{i=0}^{N}\omega_{(i)}(t)U_i(u)-\frac{1}{2}D\sum_{i=0}^{N}\left[\omega_{(i-1)}(t)+\omega_{(i+1)}(t)\right]U_i(u)\right] \\ \frac{d}{dt}\left[\sum_{i=0}^{N}y_{(i)}(t)U_i(u)\right]=\frac{1}{T_y}(k_p(r-\sum_{i=0}^{N}\omega_{(i)}(t)U_i(u))+k_i\sum_{i=0}^{N}x_{4(i)}(t)U_i(u)-k_d\frac{d}{dt}\left[\sum_{i=0}^{N}\omega_{(i)}(t)U_i(u)\right]-\sum_{i=0}^{N}y_{(i)}(t)U_i(u)) \\ \frac{d}{dt}\left[\sum_{i=0}^{N}x_{4(i)}(t)U_i(u)\right]=r-\sum_{i=0}^{N}\omega_{(i)}(t)U_i(u) \end{cases} \tag{11}$$

Let us multiply the above system of equations by $U_i(u)$. Considering the mathematical expectation with regard to the random variable *u* on both sides of Eq. (11), and setting *i*=0, 1, 2, 3, and 4, the initial probabilistic model can be approximated by the system in Eq. (12):

$$
\begin{cases}
\begin{cases}
x_{10} = x_{20} \\
x_{20} = x_{30} \\
x_{30} = -a_0 x_{10} - a_1 x_{20} - a_2 x_{30} + y_0 \\
\delta_0 = \omega_s \omega_0 \\
\omega_0 = \dfrac{1}{T_{ab}}\left[m_{t0} - E\left(\dfrac{E_q^{'} V_s}{x_{d\Sigma}^{'}} U_0(u) \sin\left(\sum_{i=0}^{N} \delta_i(t) U_i(u) \right) + \dfrac{V_s^2}{2} \dfrac{x_{d\Sigma}^{'} - x_{q\Sigma}}{x_{d\Sigma}^{'} x_{q\Sigma}} U_0(u) \sin 2\left(\sum_{i=0}^{N} \delta_i(t) U_i(u) \right) \right) - D_t \omega - \dfrac{1}{2} D \omega_1 \right] \\
y_0 = \dfrac{1}{T_y}\left(-k_p \omega_0 + k_i x_{40} - k_d \omega_0 - y_0 \right) \\
x_{40} = r - \omega_0
\end{cases} \\
\begin{cases}
x_{11} = x_{21} \\
x_{21} = x_{31} \\
x_{31} = -a_0 x_{11} - a_1 x_{21} - a_2 x_{31} + y_0 \\
\delta_1 = \dfrac{1}{2} \omega_s \omega_1 \\
\omega_1 = \dfrac{1}{T_{ab}}\left[m_{t1} - E\left(\dfrac{E_q^{'} V_s}{x_{d\Sigma}^{'}} U_1(u) \sin\left(\sum_{i=0}^{N} \delta_i(t) U_i(u) \right) + \dfrac{V_s^2}{2} \dfrac{x_{d\Sigma}^{'} - x_{q\Sigma}}{x_{d\Sigma}^{'} x_{q\Sigma}} U_1(u) \sin 2\left(\sum_{i=0}^{N} \delta_i(t) U_i(u) \right) \right) - D_t \omega - \dfrac{1}{2} D\left(\omega_0 + \omega_2 \right) \right] \\
y_1 = \dfrac{1}{T_y}\left(-k_p \omega_1 + k_i x_{41} - k_d \dfrac{d}{dt} \omega_1 - y_1 \right) \\
x_{41} = -\omega_1
\end{cases} \\
\begin{cases}
x_{14} = x_{24} \\
x_{24} = x_{34} \\
x_{34} = -a_0 x_{14} - a_1 x_{24} - a_2 x_{34} + y_4 \\
\delta_4 = \dfrac{1}{2} \omega_s \omega_4 \\
\omega_4 = \dfrac{1}{T_{ab}}\left[m_{t4} - E\left(\dfrac{E_q^{'} V_s}{x_{d\Sigma}^{'}} U_4(u) \sin\left(\sum_{i=0}^{N} \delta_i(t) U_i(u) \right) + \dfrac{V_s^2}{2} \dfrac{x_{d\Sigma}^{'} - x_{q\Sigma}}{x_{d\Sigma}^{'} x_{q\Sigma}} U_4(u) \sin 2\left(\sum_{i=0}^{N} \delta_i(t) U_i(u) \right) \right) - D_t \omega - \dfrac{1}{2} D \omega_3 \right] \\
y_4 = \dfrac{1}{T_y}\left(-k_p \omega_4 + k_i x_{44} - k_d \dfrac{d}{dt} \omega_4 - y_4 \right) \\
x_{43} = -\omega_4
\end{cases}
\end{cases}
\tag{12}
$$

The formula of the mathematical expectation of the electromagnetic torque $P_e^{'}$ can be then written as:

$$
\begin{aligned}
E\left[P_e^{'} \right] &= E\left(\frac{E_q^{'} V_s}{x_{d\Sigma}^{'}} \sin\left[\sum_{i=0}^{N} \delta_{(i)}(t) U_i(u) \right] - \frac{V_s^2}{2} \frac{x_{d\Sigma}^{'} - x_{q\Sigma}}{x_{d\Sigma}^{'} x_{q\Sigma}} \sin 2\left[\sum_{i=0}^{N} \delta_{(i)}(t) U_i(u) \right] \right) \\
&= \int_{-1}^{1} \left(\frac{E_q^{'} V_s}{x_{d\Sigma}^{'}} \sin\left[\sum_{i=0}^{4} \delta_{(i)}(t) U_i(u) \right] - \frac{V_s^2}{2} \frac{x_{d\Sigma}^{'} - x_{q\Sigma}}{x_{d\Sigma}^{'} x_{q\Sigma}} \sin 2\left[\sum_{i=0}^{4} \delta_{(i)}(t) U_i(u) \right] \right) p(u) du
\end{aligned}
\tag{13}
$$

Finally, the average response can be evaluated according to the Eq. (12):

$$\begin{cases} E\left[x_1(t,u)\right]=\sum_{i=0}^{4} x_{1(i)}(t)U_i(u)=x_{10}(t) \\ E\left[x_2(t,u)\right]=\sum_{i=0}^{4} x_{2(i)}(t)U_i(u)=x_{20}(t) \\ E\left[x_3(t,u)\right]=\sum_{i=0}^{4} x_{3(i)}(t)U_i(u)=x_{30}(t) \\ E\left[\delta(t,u)\right]=\sum_{i=0}^{4} \delta_{(i)}(t)U_i(u)=\delta_0(t) \\ E\left[\omega(t,u)\right]=\sum_{i=0}^{4} \omega_{(i)}(t)U_i(u)=\omega_0(t) \\ E\left[y(t,u)\right]=\sum_{i=0}^{4} y_{(i)}(t)U_i(u)=y_0(t) \\ E\left[x_{4i}(t,u)\right]=\sum_{i=0}^{4} x_{4i}(t)U_i(u)=x_{40}(t) \end{cases} \tag{14}$$

3. Numerical simulations

The proposed model has been applied to a case-study in order to prove the efficiency and consistency of the approach. The values adopted for the parameters involved in the computation have been selected within realistic ranges: the rated generator speed is ω_s=314; the inertia time constant of the hydro-turbine generator unit is T_{ab}=8.0; the damping factor of the generator is D_f=0.5; the transient internal voltage of the armature is $E_q^{'}$=1.35; the direct axis transient reactance is $x_{d\Sigma}^{'}$=1.15; the quadrature axis reactance is $x_{q\Sigma}^{'}$=1.474; the major relay connecter response time is T_y=0.1 and the bus voltage at infinity is V_s=1.0. The first-order partial derivative value of flow rate with respect to water head is e_{qh}=0.5; the first-order partial derivative value of torque with respect to wicket gate is e_y=1.0; the intermediate variable is e=0.7; the length of the phase of the water hammer wave is T_r=1.0; the elastic time constant of the penstock is h_w=2.0; the reference input is r=0; the proportional gain of the PID controller is k_p=2 and the integral gain of the PID controller k_i=1.

The initial values of the deterministic model of the hydraulic-mechanical-electric system (1) are

$[x_1(0), x_2(0), x_3(0), \delta(0), \omega(0), y(0), x_4(0)]$=[0.001, 0.001, 0.001, 0.001, 0.001, 0.001, 0.001].

Similarly, the initial values of the random hydraulic-mechanical-electric system (11) are

$[x_{10}(0), x_{20}(0), x_{30}(0), \delta_0(0), \omega_0(0), y_0(0), x_{40}(0)]$=[0.001, 0.001, 0.001, 0.001, 0.001, 0.001, 0.001], and $[x_{1i}(0), x_{2i}(0), x_{3i}(0), \delta_i(0), \omega_i(0), y_i(0), x_{4i}(0)]$=[0, 0, 0, 0, 0, 0, 0] ($i$=0, 1, 2, 3, 4).

3.1 Global Sensitivity

Global sensitivity aims to find sensitive factors defining as parameters which have important effect on system outputs. In this subsection, global sensitivity to generator speed is performed, and the calculation result is shown in Fig. 3. Parametric uncertainties in the established model are shown in Tab. 1.

Tab. 1 Specifications of parametric uncertainties.

Definition	Symbol	Average	Standard	Distribution
Partial derivative of the flow with turbine speed	e_{qh}	0.5	0.01	Normal
Partial derivative of turbine torque with guide vane	e_y	0.03	0.01	Normal
Partial derivative of the flow with guide vane	e_{qy}	0.2	0.01	Normal
Partial derivative of torque with turbine speed	e_h	0.18	0.01	Normal
Damping factor of generator rotor	D_t	0.5	0.01	Normal
Transient internal voltage of the armature	E_q	1.35	0.1	Normal
the rated generator speed	ω_0	314	100	Normal
Inertia time constant of the generator unit	T_{ab}	8	0.5	Normal
Direct axis transient reactance	x_d	1.15	0.01	Normal
Quadrature axis reactance	x_q	1.474	0.01	Normal
Major relay connecter response time	T_y	0.1	0.001	Normal
Bus voltage at infinity	V_s	1	0.01	Normal
Length of the phase of water hammer wave	T_r	1	0.01	Normal
Elastic time constant of the penstock	h_w	2	0.01	Normal
Proportional adjustment coefficient	k_p	2	0.01	Normal
Integral adjustment coefficient	k_i	1	0.01	Normal
Differential adjustment coefficient	k_d	2	0.06	Normal
Random intensity	D	0.08	0.0003	Normal
Control signal	r	0.01	0.003	Normal

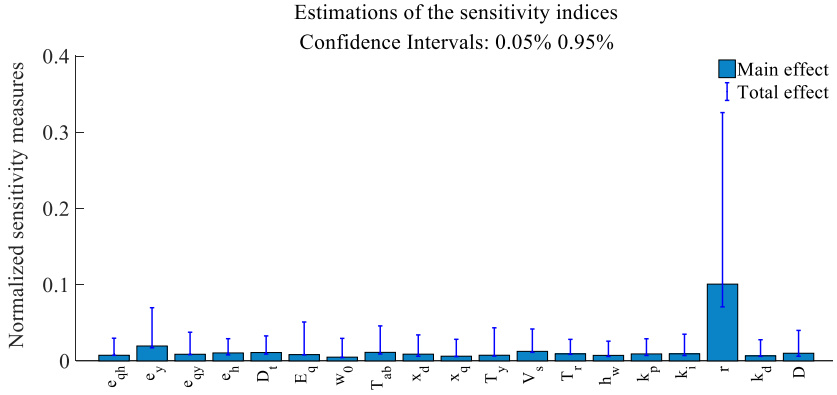

Fig. 3 Sensitivity analysis results of the generator speed.

From Fig. 3 for the generator speed, the sensitive value of control signal r is obviously larger than other parameters. In actual operating, control signal r provides a standard for generator speed, and the aim of the hydraulic generating system is regulating the guide vane opening to guarantee the generator speed changing in the required interval. Hence, control signal r playing the most sensitive parameter is very reasonable. The impact ranges of parameters in the model are summarized, which are $r > V_s > T_{ab} > D_t > e_h > D > k_i > T_r > k_p > x_d > e_{qy} > E_q > T_y > e_{qh} > h_w > k_d > x_q > w_0 > e_y$.

3.2 Dynamic evolution with different values of random intensity D

In this section, the differences between the dynamic evolution process of the generator speed ω computed with the deterministic (1) and a probabilistic approach (11) are investigated. Let the differential gain of the PID controller k_d vary between 0 and 6. According to the assumption, the dynamic evolution process of the generator speed ω can be obtained adopting the deterministic approach of Eq. (1): the results of such analysis are shown in Fig. 4(a). Similarly, Fig. 4(b) shows the results obtained adopting the probabilistic approach of Eq. (11) with regard to the generator speed. When the level of the random intensity D is 0.01, the dynamic evolution process of the generator speed ω along with increasing differential gain values k_d, assuming a random intensity D equal to 0.01.

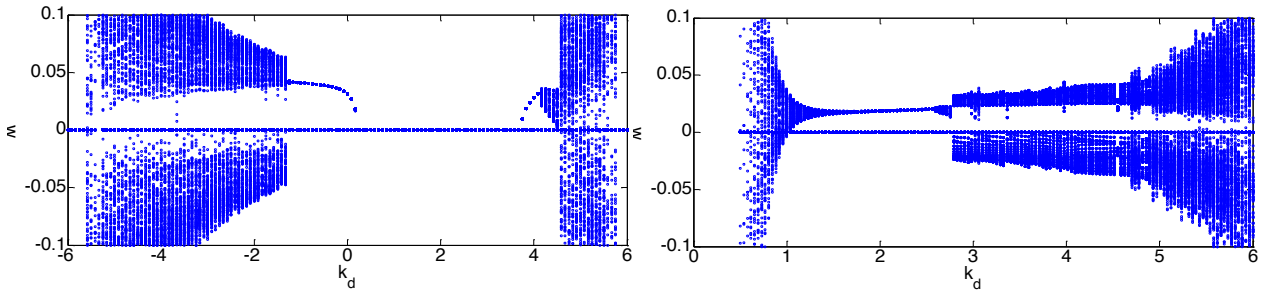

(a) Responses of the deterministic system (1) (b) D=0.01

Fig. 4 The dynamic evolution process of the generator speed ω for the deterministic approach of

Eq. (1) and the probabilistic approach shown in Eq. (11), with D=0.01 and differential gain k_d increasing from 0 to 6.

As Fig. 4(a), for k_d varying between 0 and 6, the results of the deterministic approach highlight five operating states associated with the dynamic evolution process of the generator speed ω: a random vibration state for generator speed ω within the range [-0.1, 0.1], a regular vibration state from ω=0.0188 to ω=0.02015, a stable operation state when ω is equal to zero, a quasi-periodic vibration state for values of ω lying in the interval [-0.037, 0.042], and a non-tunable state for values of ω far higher than zero. In comparison with Fig. 4(a), Fig. 4(b) shows a different dynamic evolution process of the generator speed ω when k_d changes from 0 to 6. Specifically, the differences between the two approaches can be summarized by five observations:

First, for the deterministic approach of Eq. (1), the key point (named point 1) at which the generator speed ω evolves from the non-tunable state to the random vibration state is located at k_d=-5.583. Differently, point 1 is located at k_d=0.5 for the probabilistic approach of Eq. (11).

Second, the critical point (named point 2) at which ω passes from the random vibration state to the stable operating state, moves from k_d=-1.25 to k_d=1.875 according to the adoption of the deterministic or the probabilistic approach respectively. The distance between point 1 and point 2 reveals that the adjustable range of k_d associated with the random vibration state is significantly tighter for the probabilistic case. In other words, minor changes of the value of k_d may result in the transition of the probabilistic model from the random vibration state to the non-tunable state. This transition could result in major accidents and then could have disastrous effects on the facility and its surroundings. Third, the deterministic model presents a stable state, and the corresponding adjustable range of k_d is [0.1667, 3.75]. Differently, the probabilistic model presents no stable state.

Fourth, considering the deterministic model operating in the regular vibration state, the change

rate of the generator speed is very large, while the change rate becomes quite low when the random system operates in the regular vibration state.

Fifth, with regard to the quasi periodic vibration state, the range of k_d results [4.167, 4.5] for the deterministic model and [2.563, 4.663] for the probabilistic approach.

To sum up, the results obtained with the probabilistic model do not show any stable operating state of the hydraulic-mechanical-electric system affected by the random fluctuation of the generator speed. Moreover, in comparison with the deterministic analysis, the adjustable range of k_d associated with the random vibration state is narrower, while it appears significantly wider in the right region of the domain, associated with the quasi periodic vibration state.

3.3 Definition of k_d in function of random intensity D

This section is dedicated to the study of the effects of the intensity D on the adjustable range of the differential gain k_d. Furthermore, the relation between this latter and increasing value of D is established mathematically. Fig. 5 shows the dynamic evolution of the generator speed computed with the probabilistic model of Eq.(11) for different levels of the intensity D and values of k_d within the range [0, 6].

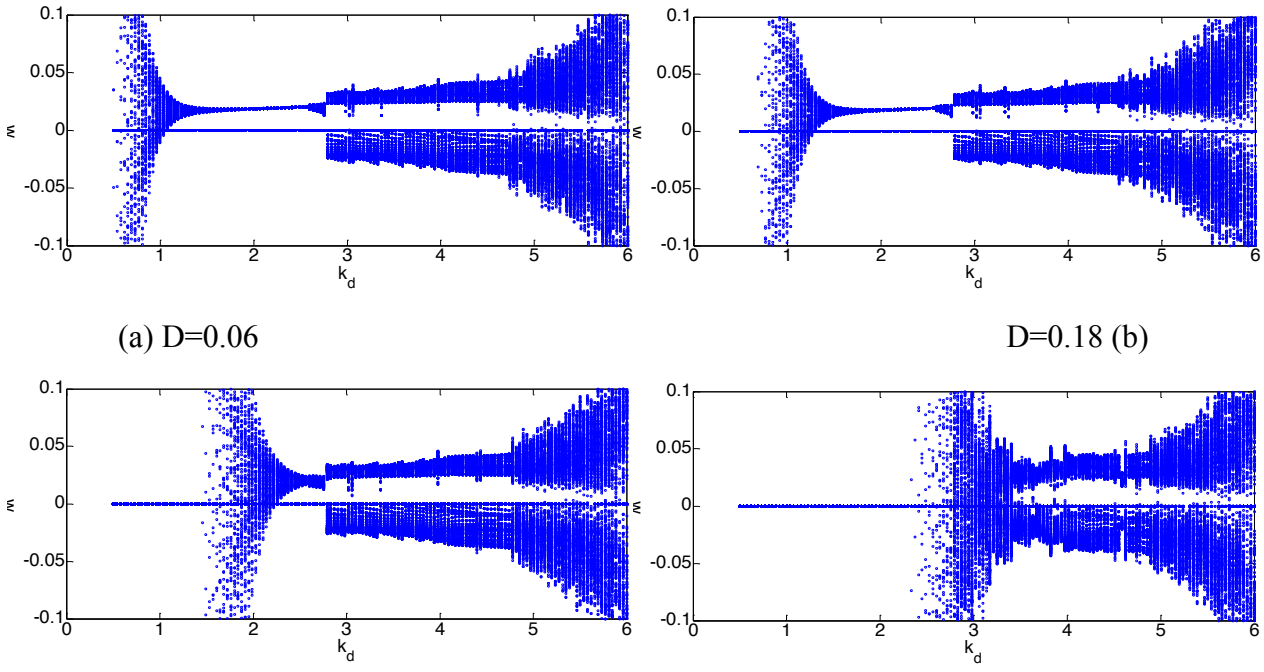

(a) D=0.06 D=0.18 (b)

(c) D=0.54 D=0.88(d)

Fig. 5 Dynamic evolution of the generator speed ω for the probabilistic model of Eq. (11) with different levels of intensity D and k_d varying from 0 to 6. (a) D=0.06; (b) D=0.18; (c) D=0.54; (d) D=0.88;

The results show that, with increasing level of the intensity D, the range of k_d which corresponds to the random vibration state on the left of point 2, does not change, as well as the operating state of the hydro-turbine generator system on the right of point 2. Conversely, the region of the k_d domain corresponding to the random vibration state and the non-tunable state shifts progressively to the right along with the increase of the intensity D. This implies that the range of k_d corresponding to the regular vibration state decreases gradually with the growth of D. When the value of D increases to 0.40, the point 2 coincides with the key point for which the system evolves from the regular vibration state to the quasi periodic vibration state. Note that, under these conditions, the range of the quasi periodic vibration state expands suddenly and the systems evolves progressively from the non-tunable state to the random vibration state and hence to the quasi periodic vibration state along the k_d domain. Under these circumstances, the severity of the system vibrations cannot be significantly decreased, regardless the entity of the adjustment applied to the value of k_d. Further, increasing the intensity D, the system shows only two possible states: the random vibrations state and the non-tunable state. Tab. 2 presents the state of the system for different values of intensity D and different ranges of k_d.

Tab. 2 Change laws of point 2 and operating ranges with increasing level of the random intensity D

D	k_d					
	State	Range	State	Range	State	range
0.01	Random vibration	(0.4236, 0.8056)	Regular vibration	(**1,875**, 2.563)	Quasi periodic vibration	(2.563, 4.663)
0.06	Random vibration	(0.4999, 0.8819)	Regular vibration	(**1.951**, 2.563)	Quasi periodic vibration	(2.563, 4.663)
0.12	Random vibration	(0.5763, 0.9583)	Regular vibration	(**2.028**, 2.563)	Quasi periodic vibration	(2.563, 4.663)

0.18	Random vibration	(0.691, 1.073)	Regular vibration	(**2.181**, 2.563)	Quasi periodic vibration	(2.563, 4.663)
0.24	Random vibration	(0.806, 1.188)	Regular vibration	(**2.257**, 2.563)	Quasi periodic vibration	(2.563, 4.663)
0.30	Random vibration	(0.958, 1.340)	Regular vibration	(**2.333**,2.563)	Quasi periodic vibration	(2.563, 4.663)
0.36	Random vibration	(1.111, 1.493)	Regular vibration	(**2.466**, 2.563)	Quasi periodic vibration	**(2.563, 4.663)**
0.42	Random vibration	(1.264, 1.646)	Regular vibration	——	Quasi periodic vibration	**(1.646, 4.663)**
0.48	Random vibration	(1.455, 1.837)	Regular vibration	——	Quasi periodic vibration	(1.837, 4.663)
0.54	Random vibration	(1.646, 2.028)	Regular vibration	——	Quasi periodic vibration	(2.028,4.663)
0.60	Random vibration	(1.799, 2.181)	Regular vibration	——	Quasi periodic vibration	(2.181, 4.663)
0.72	Random vibration	(2.142, 2.524)	Regular vibration	——	Quasi periodic vibration	(2.524, 4.633)
0.88	Random vibration	(2.792, 3.174)	Regular vibration	——	Quasi periodic vibration	(3.174, 4.633)

The results of the analysis carried out show that intensity *D* affects only the value of point 2. Moreover, this latter shifts to the right with increasing level of the intensity *D*, and for this reason the intensity D seems to have an impact on the stability of the system.

3.4 Comparison of the grid water hammer and elastic water hammer models

Technically, the penstock wall of hydropower stations is elastic. As far as the length of the penstock is less than 600 m, its shape change almost has no effect on water hammer. Thus, grid water hammer models are widely used in modeling the dynamic characteristics of small and medium hydropower stations. In this section, a comparison of the operating range between the grid water hammer and elastic water hammer models is proposed.

Subsituting the grid water hammer model with the elastic water hammer model in Eq. (1), then the hydraulic-mechanical-electric system can be rewritten as:

$$\begin{cases} \delta = \omega_s \omega \\ \omega = \dfrac{1}{T_{ab}}(m_t - \dfrac{E_q^{'} V_s}{x_{d\Sigma}^{'}}\sin\delta - \dfrac{V_s^2}{2}\dfrac{x_{d\Sigma}^{'} - x_{q\Sigma}}{x_{d\Sigma}^{'} x_{q\Sigma}}\sin 2\delta\text{-}D_t\omega - Du\omega) \\ m_t = \dfrac{1}{e_{qh}T_w}[-m_t + e_y y - \dfrac{ee_y T_w}{T_y}(k_p(r-\omega) + k_i x_4 - k_d\omega - y)] \\ y = \dfrac{1}{T_y}(k_p(r-\omega) + k_i x_4 - k_d\omega - y) \\ x_4 = r - \omega \end{cases} \tag{15}$$

Fig. 6 shows the dynamic evolution of the generator speed ω for the probabilistic model of Eq. (11), obtained by adopting the Chebyshev polynomial approximation method and computed for

different values of the intensity D and k_d varying from 0 to 6. The trend associated with point 3, namely the value of k_d for which the generator speed ω pass from the non-tunable to the vibration state, is shown in Tab. 3.

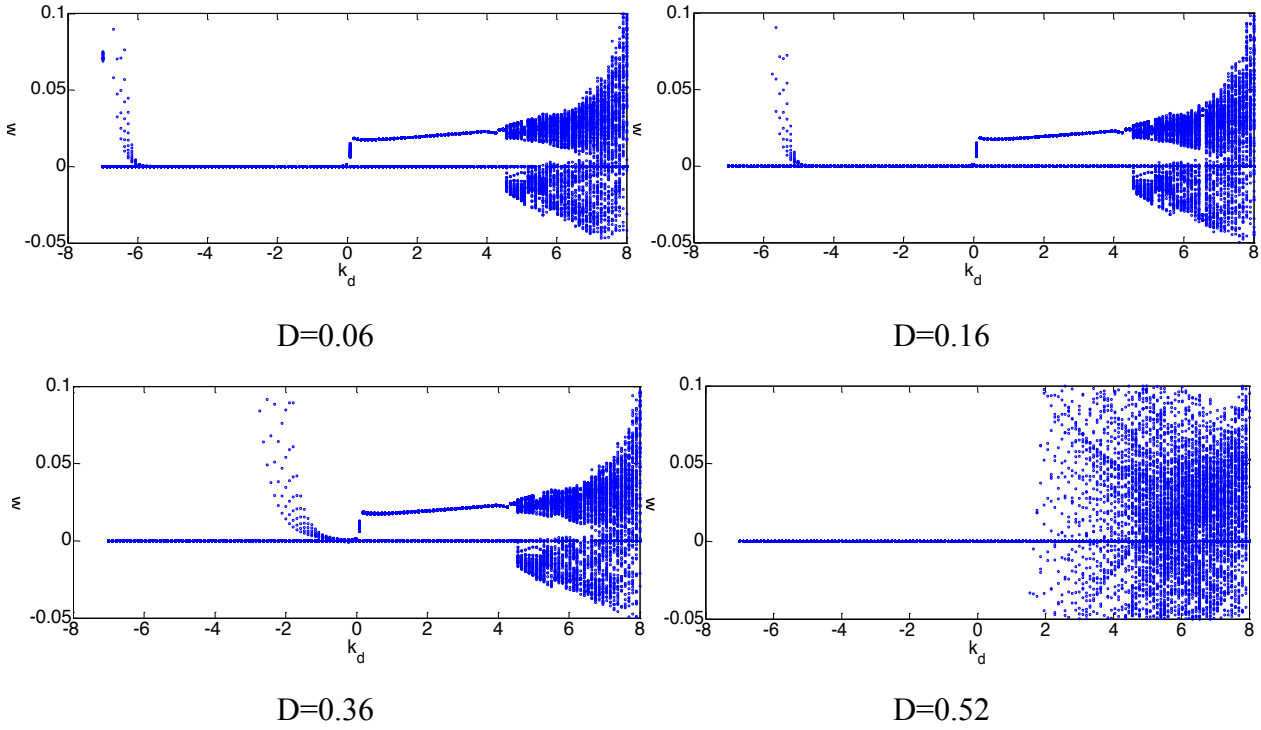

Fig. 6 Dynamic evolution of the generator speed ω for the probabilistic model in Eq. (15) with different values of the random intensity D and k_d varying from -8 to 8. (a) D=0.06; (b) D=0.16; (c) D=0.36; (d) D=0.52;

Tab. 3 Location of point 3 according to increasing values of the random intensity D

D	0.04	0.06	0.08	0.12	0.16	0.20	0.24	0.28	0.32	0.36	0.40
Point3	-5.854	-5.646	-5.542	-5.021	-4.604	-3.979	-3.25	-2.521	-1.479	-0.2292	0.083

As shown in Fig. 6 and Tab. 3, increasing levels of the intensity D cause the region of the domain associated with the non-tunable state shifting to the right, while the operating state on the right of point 3 remains unchanged. As expected, the trend registered for the probabilistic model in Eq. (15), considering the rigid water hammer model, matches perfectly the results obtained for the previous probabilistic model of Eq. (11).

In addition to this, as shown in Fig. 5(a) and Fig. 6(a), it can be noticed that when the system

operates in the regular vibration state, the amplitude of the fluctuations for the probabilistic model of Eq. (11) varies in the range of [0.0188, 0.02015], and the adjustable range of k_d is [1.951, 2.563]. Regardless of the shape changes of the penstock wall, the amplitude of the fluctuations for the probabilistic model in Eq. (15) varies in the range [0.01754, 0.02281], which is similar to the previous case. Conversely, the adjustable range of k_d, which is [0.083, 4.458], results much larger than that associated with the previous probabilistic model. Moreover, when the hydro-turbine generator unit operates in the quasi periodic vibration state, although the amplitude of the fluctuations associated with the model of Eq. (11) is similar to that of the model of Eq. (15), the range of k_d is much larger than that associated with the latter probabilistic model.

4. Conclusions

In this study, a random variable u is integrated with the generator speed of the deterministic model of a hydraulic-mechanical-electric system to establish the corresponding probabilistic model. Using this latter, the dynamic evolution of the system is analyzed, and three main conclusions can be achieved. First, although the dynamic evolution of the random system is broadly similar to that of the deterministic approach, the two sets of results show significant differences, carefully investigated in the paper. Second, the point 3, which highlights the transition from the not-tunable state to the random vibration state, shifts to the right with increasing values of the random intensity D, which leads to the decreasing adjustable range of k_d. Third, the consistence of the trends highlighted by the probabilistic model implemented in this paper is compared and verified through the use of another model. Moreover, when the shape of the penstock is assumed not uniform, the adjustable range of k_d is narrowed from left to right and the operating state of the system becomes less stable. At light of the obtained results and of the rapid development of wind power, it is recommendable to select values of the differential gain k_d of the PID governor as large as possible.

Acknowledgment

This work was supported by the scientific research foundation of National Natural Science Foundation--Outstanding Youth Foundation (51622906), National Natural Science Foundation (51479173), Fundamental Research Funds for the Central Universities (201304030577), Scientific research funds of Northwest A&F University (2013BSJJ095), Science Fund for Excellent Young Scholars from Northwest A&F University and Shaanxi Nova program (2016KJXX-55).

References

[1] Qin C, Innes-Wimsatt E, Loth E. Hydraulic-electric hybrid wind turbines: Tower mass saving and energy storage capacity. Renewable Energy. 2016;99:69-79.

[2] Chu S, Majumdar A. Opportunities and challenges for a sustainable energy future. Nature. 2012;488(7411):294.

[3] Amirante R, Cassone E, Distaso E, Tamburrano P. Overview on recent developments in energy storage: Mechanical, electrochemical and hydrogen technologies. Energy Conversion and Management. 2017;132:372–87.

[4] Simeons C. Hydro-Power1980.

[5] 2030 hydropower scale forecast: installed capacity of 450 million kilowatts generating capacity of about 1 trillion and 450 billion kwh. China Water Power & Electricfication. 2016(6):18-9. (In Chinese)

[6] Balkhair KS, Rahman KU. Sustainable and economical small-scale and low-head hydropower generation: A promising alternative potential solution for energy generation at local and regional scale. Applied Energy. 2017;188:378-91.

[7] Yazicioglu H, Tunc KMM, Ozbek M, Kara T. Simulation of electricity generation by marine current turbines at Istanbul Bosphorus Strait. Energy. 2016;95:41-50.

[8] Thiery F, Aidanpää JO. Nonlinear vibrations of a misaligned bladed Jeffcott rotor. Nonlinear Dynamics. 2016;86(3):1807-21.

[9] Quaranta E, Revelli R. Performance characteristics, power losses and mechanical power estimation for a breastshot water wheel. Energy. 2015;87:315-25.

[10] Liu X, Liu C. Eigenanalysis of Oscillatory Instability of a Hydropower Plant Including Water Conduit Dynamics. IEEE Transactions on Power Systems. 2007;22(2):675-81.

[11] Bergant A, Simpson AR, Tijsseling AS. Water hammer with column separation: A historical review. Journal of Fluids & Structures. 2006;22(2):135-71.

[12] Yang J, Wang M, Wang C, Guo W. Linear Modeling and Regulation Quality Analysis for Hydro-Turbine Governing System with an Open Tailrace Channel. Energies. 2015;8(10):11702-17.

[13] Group W. Hydraulic turbine and turbine control models for system dynamic studies. IEEE Transactions on Power Systems. 1992;7(1):167-79.

[14] Nguimdo RM, Tchitnga R, Woafo P. Dynamics of coupled simplest chaotic two-component electronic circuits and its potential application to random bit generation. Chaos. 2013;23(4):043122.

[15] Aly HHH, Mo EH. A Proposed ANN and FLSM Hybrid Model for Tidal Current Magnitude and Direction Forecasting. IEEE Journal of Oceanic Engineering. 2014;39(1):26-31.

[16] Chen D, Ding C, Do Y, Ma X, Zhao H, Wang Y. Nonlinear dynamic analysis for a Francis hydro-turbine governing system and its control. Journal of the Franklin Institute. 2014;351(9):4596-618.

[17] Afshar MH, Rohani M, Taheri R. Simulation of transient flow in pipeline systems due to load rejection and load acceptance by hydroelectric power plants. International Journal of Mechanical Sciences. 2010;52(1):103-15.
[18] Chen J, Yang HX, Liu CP, Lau CH, Lo M. A novel vertical axis water turbine for power generation from water pipelines. Energy. 2013;54(2):184–93.
[19] Gustavsson RK, Aidanpää JO. Evaluation of impact dynamics and contact forces in a hydropower rotor due to variations in damping and lateral fluid forces. International Journal of Mechanical Sciences. 2009;51(9–10):653-61.
[20] Li H, Chen D, Zhang H, Wu C, Wang X. Hamiltonian analysis of a hydro-energy generation system in the transient of sudden load increasing. Applied Energy. 2017;185:244-53.
[21] Liang J, Yuan X, Yuan Y, Chen Z, Li Y. Nonlinear dynamic analysis and robust controller design for Francis hydraulic turbine regulating system with a straight-tube surge tank. Mechanical Systems & Signal Processing. 2017;85:927-46.
[22] Nagode K, Škrjanc I. Modelling and Internal Fuzzy Model Power Control of a Francis Water Turbine. Energies. 2014;7(2):874-89.
[23] Shariatkhah MH, Haghifam MR, Chicco G, Parsa-Moghaddam M. Modelling the Operation Strategies of Storages and Hydro Resources in Adequacy Analysis of Power Systems in Presence of Wind Farms. Iet Renewable Power Generation. 2016;10(8).
[24] Xu B, Chen D, Zhang H, Wang F. Modeling and stability analysis of a fractional-order Francis hydro-turbine governing system. Chaos Solitons & Fractals. 2015;75:50-61.
[25] Wu Q, Zhang L, Ma Z. A model establishment and numerical simulation of dynamic coupled hydraulic–mechanical–electric–structural system for hydropower station. Nonlinear Dynamics. 2016:1-16.
[26] Al-Sharafi A, Sahin AZ, Ayar T, Yilbas BS. Techno-economic analysis and optimization of solar and wind energy systems for power generation and hydrogen production in Saudi Arabia. Renewable & Sustainable Energy Reviews. 2017;69:33-49.
[27] Aly HHH. Dynamic modeling and control of the tidal current turbine using DFIG and DDPMSG for power system stability analysis. International Journal of Electrical Power & Energy Systems. 2016;83:525-40.
[28] Chiang MH. A novel pitch control system for a wind turbine driven by a variable-speed pump-controlled hydraulic servo system. Mechatronics. 2011;21(4):753-61.
[29] Henriques TADJ, Hedges TS, Owen I, Poole RJ. The influence of blade pitch angle on the performance of a model horizontal axis tidal stream turbine operating under wave–current interaction. Energy. 2016;102:166-75.
[30] Kalogirou SA, Karellas S, Badescu V, Braimakis K. Exergy analysis on solar thermal systems: A better understanding of their sustainability. Renewable Energy. 2016;85:1328-33.
[31] Vaezi M, Deldar M, Izadian A. Hydraulic Wind Power Plants: A Nonlinear Model of Low Wind Speed Operation. IEEE Transactions on Control Systems Technology. 2016;24(5):1-9.
[32] Shi RJ, Fan XC, He Y. Comprehensive evaluation index system for wind power utilization levels in wind farms in China. Renewable & Sustainable Energy Reviews. 2017;69:461-71.
[33] Nagamani G, Ramasamy S. Stochastic dissipativity and passivity analysis for discrete-time neural networks with probabilistic time-varying delays in the leakage term. Applied Mathematics & Computation. 2016;289(C):237-57.
[34] Saadabad NA, Moradi H, Vossoughi G. Semi-active control of forced oscillations in power transmission lines via optimum tuneable vibration absorbers: With review on linear dynamic aspects. International Journal of Mechanical Sciences. 2014;87(4):163-78.
[35] Trivedi C, Gandhi BK, Cervantes MJ, Dahlhaug OG. Experimental investigations of a model Francis turbine during shutdown at synchronous speed. Renewable Energy. 2015;83:828-36.
[36] Thiery F, Gustavsson R, Aidanpää JO. Dynamics of a misaligned Kaplan turbine with blade-to-stator contacts. International Journal of Mechanical Sciences. 2015;99:251-61.
[37] Xu W. Numerical analysis methods for stochastic dynamical system: Science Press, 2013. (In Chinese).